Resolving discordant U–Th–Ra ages: constraints on petrogenetic processes of recent effusive eruptions at Tatun Volcano Group, northern Taiwan

GEORG F. ZELLMER[1]*, KENNETH H. RUBIN[2], CHRISTIAN A. MILLER[2], J. GREGORY SHELLNUTT[3], ALEXANDER BELOUSOV[4] & MARINA BELOUSOVA[4]

[1]*Soil & Earth Sciences Group, Institute of Agriculture & Environment, Massey University, Tennent Drive, Palmerston North 4410, New Zealand*

[2]*Department of Geology and Geophysics, SOEST, University of Hawaii, 1680 East-West Road, Honolulu, Hawaii 96822, USA*

[3]*Department of Earth Sciences, National Taiwan Normal University, 88 Tingzhou Road Sec. 4, Taipei 11677, Taiwan*

[4]*Institute of Volcanology and Seismology, 9 Piip Boulevard, Petropavlovsk-Kamchatsky, 683006, Russia*

**Corresponding author (e-mail: g.f.zellmer@massey.ac.nz)*

Abstract: U–Th–Ra isotope analyses of whole rocks and mineral separates were conducted in order to perform isochron dating of three morphologically young lavas from Tatun volcano, northern Taiwan (from Mt Cising, the Shamao dome and the Huangzuei volcano). The data do not yield tight U–Th isochrons, indicating open-system magmatic processes. However, crystallization ages of two samples can be constrained: namely, less than about 1370 years for the Shamao dome, based on ^{226}Ra–^{230}Th disequilibrium in magnetite, and less than approximately 70 ka (but potentially Holocene) for a Huangzuei flow, based on ^{238}U–^{230}Th disequilibrium in plagioclase. Discordant Ar–Ar, ^{238}U–^{230}Th and ^{226}Ra–^{230}Th ages are best explained by young lavas having inherited some crystals from older lithologies (crystal mushes or rocks), and indicate that the above ages represent maxima. Our study provides the first evidence of effusive volcanism at the Tatun Volcano Group in Late Holocene times. All separates from the Shamao dome and Huangzuei volcano are in ^{234}U–^{238}U equilibrium. Minerals in the Mt Cising sample are in ^{234}U–^{238}U disequilibrium, despite the ^{234}U–^{238}U equilibrium of the whole rock. We interpret this as uptake of a hydrothermally altered, old crystal cargo into fresh melt prior to eruption. A different dating approach will thus be required to constrain the eruption age of Mt Cising.

Supplementary material: Ar–Ar plateaus from Mt Cising and the Shamao dome, reproduced from Lee (1996), are available at www.geolsoc.org.uk/SUP18817

The Tatun Volcanic Group (TVG) is located in northern Taiwan in close proximity to Taipei City (population: 2.7 million) and its suburbs (Fig. 1), and knowledge of its volcanic history is paramount for local hazard assessments. The origin of volcanic activity in the area has been attributed to either subduction at the SW end of the Ryukyu Arc or crustal extension associated with the opening of the Okinawa Trough. Recent gas geochemical and geophysical work suggests that the magmatic system underlying the TVG remains active. For example, ^{3}He/^{4}He isotope ratios of fumaroles and hot springs in the area are elevated to magmatic values of up to 7.6 R/R_A (where R is the ^{3}He/^{4}He ratio of the sample, and R_A is the ^{3}He/^{4}He ratio of the air) (Yang *et al.* 1999; Lee *et al.* 2008), and the chemistry of some fumaroles indicate a magmatic component in their source (Lee *et al.* 2005, 2008; Witt *et al.* 2008), suggesting that magma may be degassing at depth. A high geothermal gradient of 100 °C km^{-1} (Song *et al.* 2000), local ground deformation (Yu *et al.* 1997) and the recent occurrence of volcano-seismic signals (Kim *et al.* 2005; Lin *et al.* 2005; Konstantinou *et al.* 2007) are geophysical indicators of continuing tectonomagmatic activity at depth in the area. Given the potential for future volcanic eruptions and the associated vulnerability to a range of volcanic hazards (Konstantinou 2015), it is critical to gain a better understanding of the timing and duration of TVG volcanic activity.

From: Caricchi, L. & Blundy, J. D. (eds) *Chemical, Physical and Temporal Evolution of Magmatic Systems*. Geological Society, London, Special Publications, **422**, http://doi.org/10.1144/SP422.3

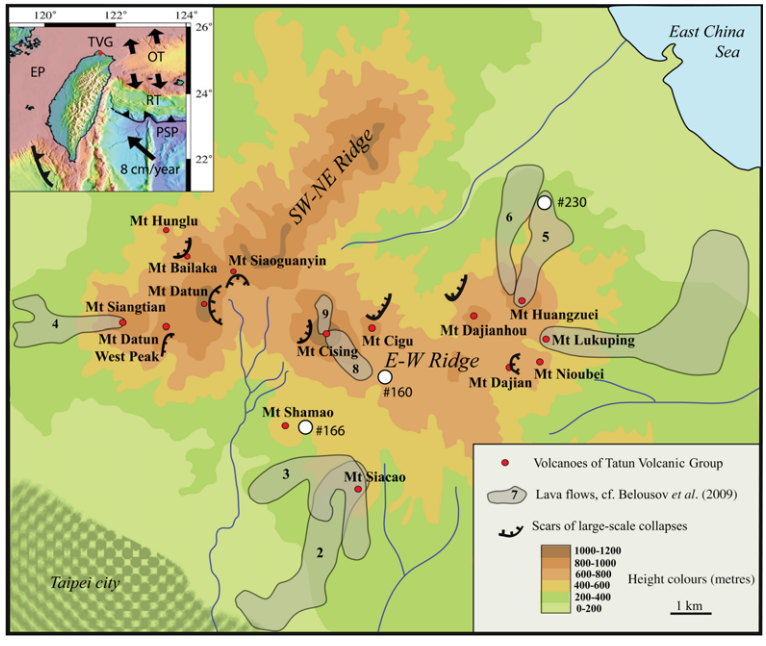

Fig. 1. Sketch map of the Tatun Volcanic Group (TVG), northern Taiwan, adapted from Belousov *et al.* (2010). Locations of the main volcanic ridges, volcanoes, lava flows and collapse scars are shown. White dots indicate sampling sites. The location of the TVG, as well as the tectonic regime of Taiwan, is provided in the inset. EP, Eurasian Plate; PSP, Philippine Sea Plate; OT, Okinawa Trough; RT, Ryukyu Trench.

K–Ar and Ar–Ar dating suggest that volcanism started at around 2.8 Ma and lasted until about 0.2 Ma, with the youngest ages determined on some of the morphologically most pristine deposits (Song *et al.* 2000). However, approximately 20 kyr-old tephra deposits found within the Taipei basin (Wang-Lee *et al.* 1978) suggested a potentially much younger age of explosive volcanic activity. Belousov *et al.* (2010) corroborated this notion with ^{14}C ages of several young TVG tephras, yielding ages between 23 and 13 ka, and an even younger phreatic eruption as recently as about 6 ka. Such recent explosive activity raises some doubt about the validity of the youngest Ar–Ar ages of TVG effusive eruption deposits. For example, Belousov *et al.* (2010) indicated that the youngest of the obtained Ar–Ar dates of around 0.2 Ma (Lee 1996) may have been affected by slight contamination through admixing of older xenocrysts originating from Miocene Sandstones underlying the area.

The present study was conducted to provide independent age constraints on some of the youngest effusive eruptions of the TVG through U–Th internal isochron dating (e.g. Pyle *et al.* 1988; Bourdon *et al.* 1994; Turner *et al.* 2000; Condomines *et al.* 2003; Zellmer *et al.* 2008) and ^{226}Ra–^{230}Th magnetite dating (cf. Rubin & Zellmer 2009 and references therein). On the basis of the new U-series data, we here discuss petrogenetic processes, age constraints and implications for hazard-mitigation at Tatun volcano.

Sample background

Sample selection

Three hornblende-bearing volcanic samples were collected for U-series internal isochron work by two of us (AB and MB) during fieldwork in 2008–2009. Details on sampling location and sample types are provided in Table 1. Samples were chosen for U-series dating on basis of the morphologically young character of the respective deposits. Mt Cising and the Shamao dome yield Ar–Ar ages of 0.72 ± 0.04 and 0.23 ± 0.01 Ma, respectively (Lee 1996), and Mt Huangzuei yields a K–Ar age of 0.22 ± 0.02 Ma (Tsao 1994). Although U–Th and Ra–Th dating are limited to samples younger than about 350 and 8 ka, respectively, there was some doubt about the accuracy of the Ar–Ar and K–Ar ages: Ar–Ar age plateaus were not very well defined, and admixing of older xenocrysts was considered a possibility (Belousov *et al.* 2010). The morphologically young character of the deposits suggested that eruption ages may be significantly

Table 1. *Sample details*

Volcano	Sample	Northern latitude	Eastern longitude	Elevation (m)	Comment
Mt Cising	#160	25°09′26.6″	121°34′01.2″	567	Block from lahar deposit, probably connected to flow #8 in Figure 1
Mt Shamao	#166	25°08′51.8″	121°33′04.5″	372	Lava dome sample
Mt Huangzuei	#230	25°11′30.3″	121°36′25.0″	312	Sample taken from flow #5 in Figure 1

younger and, thus, within the range of the U-series dating method.

Geochemical overview

The details of the major- and trace-element chemistry of these rocks and their relationship to other TVG samples is discussed elsewhere (Shellnutt *et al.* 2014) and only briefly summarized here. Following the classification schemes of Peacock (1931), Peccerillo & Taylor (1976) and Arculus (2003), the samples investigated here are medium-K, medium-Fe, calcic basaltic andesites and andesites. All samples are enriched in large ion lithophile trace elements, in light rare earth elements (REEs) relative to heavy REEs, and show negative spikes in Ta, Nb and Ti (Fig. 2). This signature is typical for magmas generated from a subduction-modified mantle source (e.g. Gill 1981). The andesitic samples studied here have some adakitic affinities given their high Sr/Y and La/Y ratios, low HREE content, and their lack of negative Eu anomalies (cf. Defant & Drummond 1990). However, relatively flat middle to heavy REE patterns suggest that there is no significant control of residual garnet during the genesis of these melts. Our whole-rock results are consistent with previous work on the geochemistry of volcanic rocks from the northern Taiwan region (Wang *et al.* 2004), and indicate that the samples studied here are geochemically typical TVG eruptives.

Mineralogical and petrographical features

The mineralogy and petrographical features of the analysed samples are seen in thin-section photographs taken in plane-polarized and cross-polarized light (Fig. 3). All samples are porphyritic, and contain plagioclase, magnetite, amphibole and pyroxene. The sample from Mt Cising has relatively few large pyroxene crystals; its major phase assemblage is dominated by plagioclase, amphibole and large magnetite crystals. The Shamao dome sample has magnetite both within the groundmass and as large inclusions within amphibole and pyroxene. The Huangzuei sample is dominated by plagioclase and magnetite, with amphibole and pyroxene typically only occurring as microphenocrysts and in the groundmass. All samples show disequilibrium features such as complexly zoned and sieve-textured

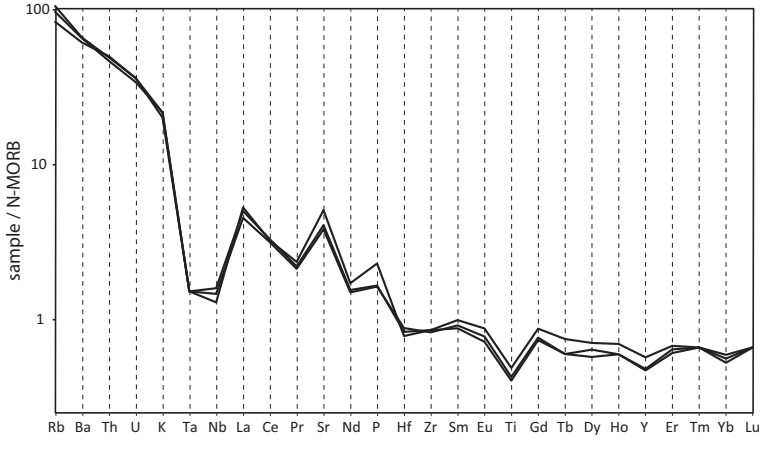

Fig. 2. Multi-element spidergram of the studied TVG whole-rock samples, normalized to normal-type mid-ocean ridge basalt (N-MORB) (Sun & McDonough 1989).

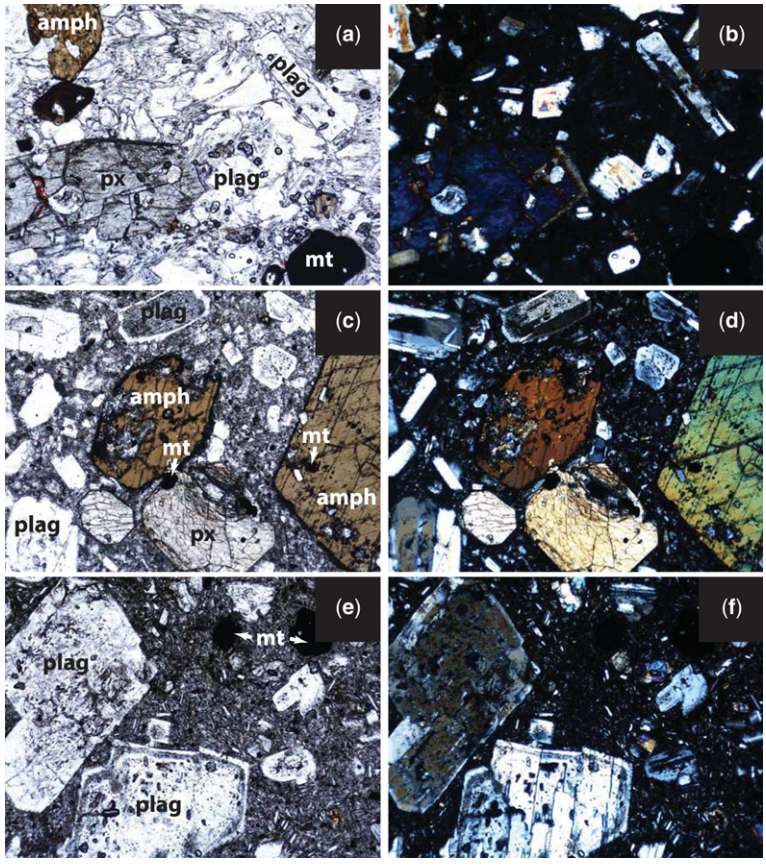

Fig. 3. Petrographical images of analysed samples from the TVG. Field of view is 3 mm in diameter on each photograph. (**a**) Plane-polarized light (PPL) and (**b**) crossed-polarized light (XPL) images of sample #160 from Mt Cising. Note that this sample contains only few large pyroxene crystals, of which one is seen in the image. Plagioclase, amphibole and magnetite dominate the phase assemblage. (**c**) PPL and (**d**) XPL images of sample #166 from Mt Shamao. Note magnetite is often present as inclusions within amphibole and pyroxene in this sample. (**e**) PPL and (**f**) XPL images of sample #230 from Mt Huangzuei. Note that large crystals are dominated by magnetite and plagioclase, while amphibole and pyroxene are restricted to the groundmass. amph, amphibole; mt, magnetite; plag, plagioclase; px, pyroxene.

plagioclase crystals, amphiboles with pronounced oxidation rims, and resorbed and fractured crystals. Such textures are commonly observed in magmas from subduction-zone environments, and are typical for minerals that have not formed from the melt they are carried in. The possibility of crystal inheritance or uptake thus needs to be kept in mind when internal isochron dating is performed on these samples.

Analytical techniques

Analysis of U and Th concentrations in whole rocks and separates

Mineral separation was undertaken at Chengxin Geological Services Co. Ltd, Langfang City, PRC, to obtain gram quantities of highly pure mineral separates. Details of the separation procedures are provided in Zellmer *et al.* (2014*a*). U-series and radiogenic isotope analysis were conducted in the SOEST isotope laboratory of the University of Hawaii at Manoa. To minimize differences in analysis conditions, we optimized sample sizes and split fractions to provide roughly constant analyte quantities of 50–100 ng for U and Th, using whole-rock concentration data and qualified estimates for the mineral separates. All wet chemical procedures were conducted in a clean room with ultra-pure reagents prepared in-house. HCl and HNO_3 were quartz distilled, while HF was purified with a two-bottle Teflon still. Reagents contained 0.01–1 pg g^{-1} Th and U, and undetectable Ra. Procedural blanks were <5 pg for the full Th–U analytical

procedure and undetectable for Ra. Whole-rock powders and phenocryst separates (except magnetite) were washed multiple times in ultra-pure water prior to drying, weighing and complete digestion/dissolution with $HF-HNO_3$, and dissolved into HNO_3. Solutions were centrifuged to ensure complete dissolution. These procedures have previously been demonstrated to result in complete sample dissolution of mafic compositions, and were checked by replicate analyses of rock standard K1919 and interlaboratory checks on unknown samples (Rubin *et al.* 2005). Magnetite separates were treated similarly except that dissolution was carried out with aqua regia in microwavable Teflon bombs. After dissolution, all samples were split into Th–U isotopic composition (IC) and Th–U isotopic dilution (ID) aliquots, and the ID aliquots were spiked with a calibrated $^{229}Th-^{233}U$ tracer. Th and U were separated and purified using previously described anion-exchange methods (Rubin *et al.* 2005). Analytical blanks are $\leq 0.1\%$ for Th and U (typically 1–2 pg).

For measurement of U and Th concentrations by ID, we employed thermal ionization mass spectrometry (TIMS) (using a Sector 54-WARP) of Th and U loaded onto colloidal graphite on Re filaments (Rubin *et al.* 2005). Reported uncertainties for ID analyses reflect fractional errors of data acquisition (2σ standard errors of 30–50 ratios), weighing and spike calibration. External precision as 2σ variation about the mean for ^{238}U and ^{232}Th ID analyses have been previously established by replicate dissolution analyses ($n = 7-12$) to be 0.5% (Rubin *et al.* 2005).

Analysis of Th isotopic compositions in whole rocks and separates

The Th IC analysis employed a late-model, second-generation Nu Plasma 'HR' multicollector inductively coupled plasma (ICP) mass spectrometer at the University of Hawaii at Manoa, with 6 kV accelerating voltage and with a retardation filter fitted in front of the ion counter used for ^{230}Th analyses ('IC0'). After chemical separation/purification, Th IC samples were taken up into a known mass of 5% HNO_3 solution and quickly evaluated for ^{232}Th intensity using a three-point calibration curve. Samples were then taken up into a volume of solution necessary to result in a Th concentration of 10 ppb (and 5 ppb U, which is used for internal gain calibration and mass bias corrections). All Th (and U) isotopic analyses utilized a Nu Instruments 'DSN-100' desolvating nebulizer, plus dry plasma cones and an S-option vacuum pump fitted on the mass spectrometer.

At the beginning of each analytical session, Faraday detector gains were determined, followed by Th tail analysis (that was sometimes also done at the end), using standard solutions at 5, 10, and 20 ppb Th (all also containing 5 ppb U). These were used to evaluate the ^{232}Th tail contribution on mass 230. Intensities were taken at masses 232, 231, 230.5, 229.5, 228.5 and 227.5 amu. An exponential function was then fitted to the 231, 230.5, 229.5, 228.5 and 227.5 amu data to model the ^{232}Th tail and to allow the interpolation of the tail at 230 amu. These interpolated values were averaged over all three (or six) analyses and expressed on a ^{232}Th normalized basis (i.e. cps of the ^{232}Th tail at mass 230 per volt of signal at mass 232). The ^{232}Th tail values did not change substantially during the course of the analyses.

Samples were analysed by standard-sample bracketing using a series of four Th isotopic gravimetric standards (named 'Hawaii-Th-A'–'Hawaii-Th-D') prepared 'in-house' and calibrated against UCSC Th 'A' by bracketing analysis using a $^{232}Th/^{230}Th$ value of $170{,}761 \pm 0.08\%$ $2\sigma_m$, $n = 255$ (Rubin 2001). Which bracketing standard was employed for a given sample was decided based on expected $^{232}Th/^{230}Th$ ratios, based in turn on Th/U ratios of the samples. All bracketing standards and unknown samples were doped to 5 ppb U. A 7 min rinse with 5% HNO_3 was conducted between analyses of bracketing standards and unknown samples, sufficient to reduce the ^{232}Th intensity to <2 mV, compared to about 1.5–2 V of ^{232}Th during analysis. Each bracketing-standard and unknown-sample run took about 21 min and consisted of 75 measurements (three blocks of 25 measurements each). Each block included a zero measurement taken at $+0.5$ amu. Each measurement consisted of two cycles: the first cycle measured ^{235}U on IC0 and ^{238}U on L2 for 3 s; and the second cycle measured ^{230}Th on IC0, ^{232}Th on L3, ^{235}U on the axial and ^{238}U on H3 for 5 s. After each magnet jump, the magnet was allowed to settle for 2 s.

Within-run data reduction for each bracketing standard and unknown sample included: (a) an IC0 gain relative to the Faradays calculated using the ^{235}U and ^{238}U data from both cycles; this gain (typically *c.* 75%) was applied to the raw ^{232}Th and ^{230}Th voltage data to give a gain-corrected $^{232}Th/^{230}Th$ ratio; and (b) an internal mass bias correction of the gain-corrected $^{232}Th/^{230}Th$ ratios using the measured $^{238}U/^{235}U$ ratio and the accepted value of 137.837 (Richter *et al.* 2010).

During subsequent off-line data reduction, the Th isotopic data from each analytical session (bracketing standards and unknowns) were tail-corrected with the session-specific correction (e.g. Pietruszka *et al.* 2002), after which unknown sample data were corrected for mass bias using the internal U standard, and by standard bracketing using data

obtained immediately before and after that sample. Exponential 'β'-correction factors (e.g. Hoffmann *et al.* 2007) for each preceding and following bracketing-standard analysis were determined from the tail- and gain-corrected $^{232}Th/^{230}Th$ ratios for each standard and compared to the 'true value' of this standard. These correction factors from the bracketing standards were then averaged and applied to the intervening tail- and gain-corrected $^{232}Th/^{230}Th$ ratios of the unknown sample.

Reported uncertainties for Th IC analyses reflect data acquisition errors only (i.e. they do not include half-life errors). External precision as 2σ variation about the mean of replicate dissolutions of K1919 ($n = 7$) is $\pm$ 0.8%.

Analysis of U isotopic compositions in whole rocks and separates

The U IC analysis was undertaken using the same Nu Plasma HR mass spectrometer at the University of Hawaii at Manoa, using the aforementioned dry plasma conditions. Prior to analysis, U IC samples were taken up into a known mass of 5% HNO_3 solution, and quickly evaluated for ^{238}U intensity using a three-point CRM112a calibration curve. Samples were then taken up into a volume of solution necessary to result in a U concentration of 5 ppb, a level that allowed internal gain correction by cross analysis of ^{235}U on IC0 and the Faraday detector.

Samples were run using bracketing-standard solutions of CRM112a (or, less frequently, U010). Both standards have known $^{235}U/^{238}U$ and $^{234}U/^{238}U$ ratios, but those of CRM112a are more precisely known (Richter *et al.* 2010). A 7 min washout rinse with 5% HNO_3 was conducted between analyses of bracketing standards and unknown samples, sufficient to reduce the ^{238}U intensity to <1‰ of its intensity during a standard or sample run. Each bracketing-standard and unknown-sample run took about 18 min and consisted of 66 measurements (three blocks of 22 measurements each). Each measurement consisted of two cycles. Peak centring on ^{238}U was performed for each of the two cycles at the beginning of every block. Zero measurements for baseline correction were taken for 10 s at the beginning of each block. Zeros were performed by electrostatic-analyser (ESA) deflection. The first cycle measured ^{238}U on Faraday detector L1, ^{235}U on L5 and ^{234}U on IC0 for 5 s. The second cycle measured ^{238}U on L2 and ^{235}U on IC0 for 3 s. After each magnet jump, the magnet was allowed to settle for 2 s.

Within-run data reduction included: zero-correction for each bracketing standard and unknown sample, followed by calculation of an exponential per-amu fractionation factor (β) calculated using the measured $^{235}U/^{238}U$ ratios from the second cycle, and the IC0 gain calculated for each $^{234}U/^{238}U$ ratio result using the measured $^{235}U/^{238}U$ ratios calculated from zero-corrected voltages from both cycles. The measured $^{234}U/^{238}U$ ratio was then zero-corrected, gain-corrected and mass-bias-corrected. Corrected $^{234}U/^{238}U$ ratios that were outside 2 standard deviations from the mean were discarded, and new means, standard deviations and standard errors were then calculated.

During external data reduction, each of the unknown sample runs was corrected to bracketing-standard data using linear correction factors determined from the average for each preceding and following standards. The corrected $^{234}U/^{238}U$ atom ratio of the sample was finally converted to activity ratios using the ^{234}U and ^{238}U half-lives of 245 620 $\pm$ 260 years and (4468.3 $\pm$ 2.4) $\times$ 10^6 years, respectively (Jaffey *et al.* 1971; Cheng *et al.* 2013).

The uncertainty of the $^{234}U/^{238}U$ atom ratio at secular equilibrium is 1.2‰ for our data set, as propagated from the uncertainties in the decay constants, calculated from the uncertainties in the reported half-lives. The uncertainty of the $^{234}U/^{238}U$ ratio for most samples in the data table is estimated by repeat measurements. Where replicates were not run, we used 2 standard deviations of 12 analyses of a K1919 solution, which is 6.5‰. $^{234}U-^{238}U$ disequilibria were identified when the sample ($^{234}U/^{238}U$) activity ratio deviated from unity by more than the combined equilibrium and sample uncertainties.

Analysis of ^{226}Ra concentrations in whole rocks and separates

^{226}Ra concentration was measured in one whole rock and one magnetite separate by ID TIMS using previously described methods (Rubin *et al.* 2005; Zellmer *et al.* 2008). Isotope dilution used a calibrated ^{228}Ra spike (in this case, Hawaii-Ra-spike #3) that was milked from a ^{232}Th solution and calibrated against NIST SRM 4966. Ra and Ba were separated from the sample, following the Th–U separation, by removal from the cation wash cut of the Th–U anion column. This was followed by purification of Ra (and removal of Ba) using Eichrom Sr-Resin, and removal of organic matter from the eluent using Eichrom pre-filter material and refluxing of solutions in a 50–50 mix of 30% H_2O_2 and 8N HNO_3. Samples were loaded onto Ta_2O_5 fines on outgassed W filaments, and analysis was conducted on an ion-counting Daly detector Sector 54 thermal ionization mass spectrometer (at the University of Hawaii) at filament temperatures of 1400–1550 °C and ^{226}Ra count rates of 250–500 cps.

Table 2. *U–Th–Ra compositions of whole rocks and separates*

Sample	Phase*	U ($ng\ g^{-1}$)	$\pm 2\sigma$	Th ($ng\ g^{-1}$)	$\pm 2\sigma$	Ra ($fg\ g^{-1}$)	$\pm 2\sigma$	($^{234}U/^{238}U$)	$\pm 2\sigma$	($^{238}U/^{232}Th$)	$\pm 2\sigma$	($^{230}Th/^{232}Th$)	$\pm 2\sigma$	($^{226}Ra/^{230}Th$)	$\pm 2\sigma$
Mt Cising volcano															
#160	wr	1678	2.1	5302	8.8	–	–	0.998	0.007	0.960	0.002	0.899	0.008	–	–
	plag	691	0.7	1926	3.4	–	–	0.974	0.003	1.088	0.002	1.292	0.011	–	–
	mt	246	0.2	697	1.0	–	–	1.010	0.003	1.074	0.002	1.151	0.010	–	–
	amph	211	0.5	651	1.3	–	–	0.987	0.009	0.983	0.003	0.970	0.008	–	–
Mt Shamao volcano															
#166	wr	1619	1.4	5067	6.1	522.4	3.4	1.001	0.007	0.969	0.001	0.919	0.008	1.008	0.006
–	plag	213	0.6	667	1.8	–		0.998	0.007	0.967	0.004	1.060	0.009	–	–
–	mt	671	0.5	898	0.9	56	0.7	0.996	0.007	2.267	0.003	1.257	0.011	0.447	0.005
–	amph	209	0.7	609	0.7	–	–	1.003	0.007	1.044	0.004	0.978	0.008	–	–
–	px	209	0.2	672	0.6	–	–	1.004	0.007	0.942	0.001	0.908	0.008	–	–
Mt Huangzuei volcano															
#230	wr	1626	1.3	5168	5.9	–	–	0.996	0.007	0.955	0.001	0.956	0.010	–	–
–	gm	1992	1.9	6335	8.1	–	–	0.999	0.007	0.954	0.002	0.954	0.010	–	–
–	plag	281	1.3	541	1.1	–	–	1.002	0.004	1.580	0.008	1.257	0.009	–	–
–	mt	389	0.4	822	1.0	–	–	0.998	0.003	1.438	0.002	1.313	0.009	–	–

*amph, amphibole; gm, groundmass. mt, magnetite; plag, plagioclase; px, pyroxene; wr, whole rock.

Results

U–Th ID and IC data are reported in Table 2 and plotted on U–Th equiline diagrams in Figures 4 and 5. All whole-rock (wr) samples plot in or close to $^{238}U-^{230}Th$ equilibrium at ($^{230}Th/^{232}Th$) activity ratios of between 0.90 and 0.96. At Huangzuei volcano, where a groundmass (gm) separate was analysed, whole-rock and groundmass ICs are identical. Several mineral separates display U–Th disequilibria. U excess dominates, but Th excesses are observed for a plagioclase separate from the Shamao dome, and for plagioclase and magnetite separates of Mt Cising. All mineral separates of Mt Cising (sample #160) also show small $^{234}U-^{238}U$ disequilibria (cf. Table 2), in contrast to the Mt Cising whole rock. All other samples are in $^{234}U-^{238}U$ equilibrium. Internal U–Th ages can be determined for mineral–mineral pairs from the Shamao dome and mineral–groundmass pairs from Huangzuei volcano. The Shamao dome yields a pyroxene–wr–magnetite age of 33.2 ± 1.3 ka (2σ), an amphibole–magnetite age of 28.3 ± 1.5 ka (2σ) and a plagioclase–magnetite age of 18.0 ± 1.3 ka (2σ). An amphibole–pyroxene–wr errorchron of $133 + 51/-35$ ka (2σ) has low precision due to insufficient U–Th fractionation of these phases, and yields an initial ($^{230}Th/^{232}Th$) activity ratio of 0.81 ± 0.37 (omitted from Fig. 5a for clarity). Huangzuei volcano yields a plagioclase–wr/gm age of 72 ± 4 ka (2σ) and a magnetite–wr/gm age of 148 ± 10 ka (2σ). ^{226}Ra data have been obtained for the Shamao dome whole rock and the Shamao magnetite separate. The whole rock is close to secular equilibrium, with a ($^{226}Ra/^{230}Th$) activity ratio of 1.008 ± 0.006 (2σ). In contrast, the magnetite separate displays strong ^{226}Ra-depletion, with a ($^{226}Ra/^{230}Th$) activity ratio of 0.447 ± 0.005 (2σ). As the partitioning of Ra into magnetite is extremely low due to the large size of the Ra^{2+} cation (Blundy & Wood 2003), the initial amount is negligible: that is, all ^{226}Ra in magnetite can essentially be considered as radiogenic (Rubin & Zellmer 2009). The data thus yield a Late Holocene magnetite crystallization age for the Shamao dome of 1367 ± 11 years (2σ) (cf. Fig. 6). Discordant U–Th and Ra–Th ages are common in subduction-zone volcanics (Zellmer *et al.* 2005), and imply the mixing of old and young crystal populations. As discussed below, eruption ages of Shamao and Huangzuei are thus younger than all of their respective U-series ages.

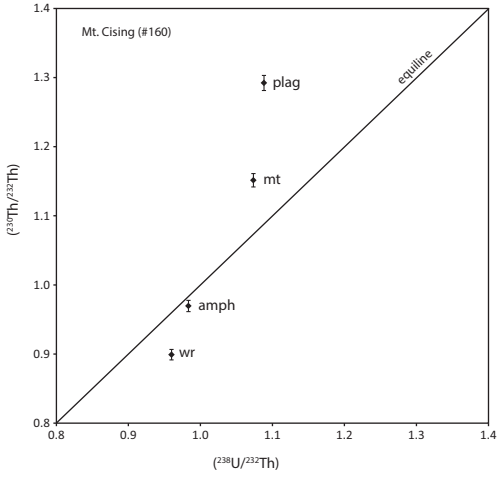

Fig. 4. U–Th equiline diagram of the Mt Cising separates. ($^{238}U/^{232}Th$) analytical uncertainties are smaller than the symbol size. Whole rock (wr), amphibole (amph), magnetite (mt), and plagioclase (plag) have been analysed.

Discussion

None of the Tatun samples we have studied yield well-behaved U–Th internal isochrons (i.e. all mineral phases lying on a single line with $0 \leq$ slope ≤ 1 on the equiline diagram). Nevertheless, important magmatic timing and petrological constrains can be determined from them. In this section, we discuss the implications of the U–Th–Ra isotope data for the petrogenetic processes operating at the TVG, and the reliability of the mineral–mineral and mineral–groundmass ages obtained for some separates. As evident from Figure 4, Mt Cising separates form a trend with a slope >1 on the equiline diagram. The minerals of the Cising sample display small $^{234}U-^{238}U$ disequilibria, while the whole-rock sample does not. This suggests that the groundmass of this sample, which hosts most of the uranium, is in $^{234}U-^{238}U$ equilibrium. However, if $^{234}U-^{238}U$ disequilibria are due to late-stage hydrothermal alteration, it is difficult to envisage how mineral alteration could have occurred without any effect on the groundmass. Zellmer *et al.* (2014*a*) recently observed very similar U–Th systematics in some southern Andean arc magmas, and interpreted the combination of fresh groundmass and altered mineral phases to represent the uptake of hydrothermally altered minerals from earlier intrusives into a fresh ascending melt prior to eruption. In Figure 7a, we have plotted the relative proportions of (^{238}U), (^{234}U) and (^{230}Th) activities of our samples, following the approach of Rosholt (1982), together with the field of data displayed by the Andean samples. It is evident that the Mt Cising minerals show significantly lower $^{234}U-^{238}U$ disequilibria than some of the mineral phases of the Andean samples. Nevertheless, it is

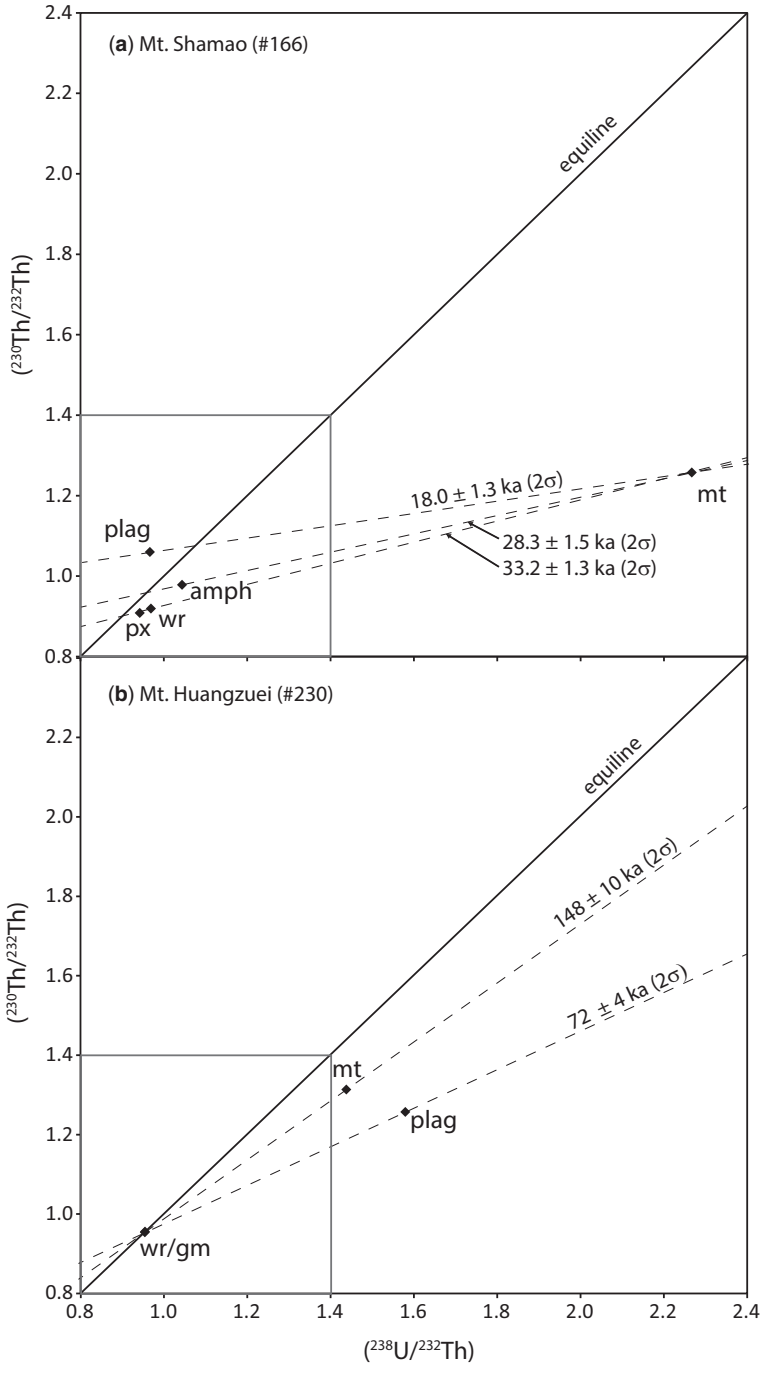

Fig. 5. U–Th equiline diagrams of (**a**) Mt Shamao separates and (**b**) separates from lava flow #5 of Mt Huangzuei. Analytical uncertainties are smaller than the symbol size. gm, groundmass; px, pyroxene; all other abbreviations are as in Figure 4. Note the expanded scale compared to Figure 4 (cf. grey outlines).

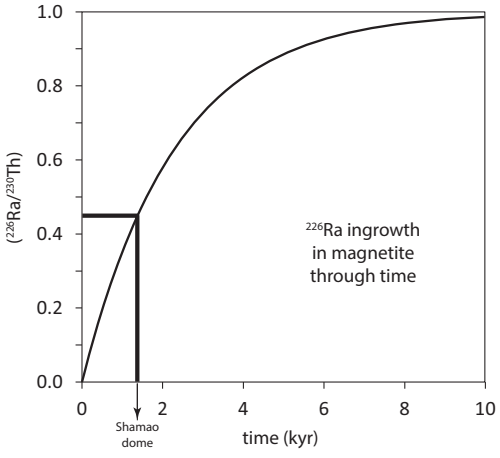

Fig. 6. Ingrowth curve of ^{226}Ra in magnetite through time. A measured (^{226}Ra/^{230}Th) activity ratio of the Shamao magnetite separate yields a time of 1367 $\pm$ 11 years (2σ).

likewise apparent that the Mt Cising minerals have been affected by small but variable amounts of uranium assimilation, ^{234}U recoil loss and ^{230}Th-predominant recoil gain processes (Fig. 7b). We would therefore argue that the crystal cargo of Mt Cising consists at least partially of hydrothermally altered material that was picked up into the fresh melt prior to, or at the onset of, the Mt Cising eruption. Cannibalization of older crystals through rising melts seems to be very common in the subduction zone environment, as has been shown using a wide range of different geochemical, mineral chemical and petrographical approaches (Stewart *et al.* 1996; Dungan 2005; Davidson *et al.* 2007; Streck *et al.* 2007; Jerram & Martin 2008; Zellmer *et al.* 2014*a*, *b*, *c*).

If crystal uptake is operating at the TVG, the impact on the 'ages' of the mixed mineral population, and the extent to which it disrupts an internal U–Th isochron of phases that did grow from the magma, needs careful consideration. The mineral assemblage of the Shamao dome (Fig. 5a) shows that some of the phases cannot be related through a simple, concomitant crystallization event. Plagioclase does not form an isochronal relationship with the whole rock, suggesting that this phase is unrelated to the magma with which it erupted. The amphibole–pyroxene–wr errorchron of 133 + 51/−35 ka (2σ) yields an age that is distinctly younger than the Ar–Ar age of 230 $\pm$ 10 ka, but is of the same order of magnitude, and the large uncertainties in interpreting the U-series in this way do not lend confidence to a potentially younger age for this dome.

However, magnetite shows the greatest U–Th disequilibrium of all phases and, because some magnetite occurs included in larger amphibole and pyroxene crystals (cf. Fig. 3c), mineral–mineral isochrons with magnetite may provide more reliable age information. A magnetite–pyroxene–wr isochron yields an age of 33.2 $\pm$ 1.3 ka (2σ), and a magnetite–amphibole isochron yields an age of 28.3 $\pm$ 1.5 ka (2σ). If the crystals providing these ages are related to the melt in which they are carried, then their true crystallization age from the melt would be around 30 ka. However, if the crystals were instead cannibalized from a previous intrusive episode, their age would be somewhat less well constrained. Given the fairly tight clustering of the whole-rock and groundmass data of all three samples around the equiline at (^{230}Th/^{232}Th) activity ratios between 0.90 and 0.96, it is likely that this represents the approximate (^{230}Th/^{232}Th) initial ratio of the TVG in general. All U/Th ratios of the Tatun whole-rock samples measured by solution inductively coupled plasma mass spectrometry (ICP-MS) suggest (^{238}U/^{232}Th) activity ratios of above 0.85 (Shellnutt *et al.* 2014). As whole rocks exclusively plot close to the equiline, this implies similar (^{230}Th/^{232}Th) activity ratios. Further, the presence of melts with (^{230}Th/^{232}Th) activities above 1 is indicated by the Shamao dome plagioclase in the Th excess.

A magnetite U–Th crystallization age range of around 20–35 ka maximum is hence yielded for any reasonable range of U–Th melt compositions generated beneath the Tatun volcano. However, if some of the crystals are inherited from an older intrusive episode, the age of eruption may be younger still. We have tested this by obtaining ^{226}Ra data for the Shamao whole rock and magnetite separate. While the whole rock is close to ^{226}Ra–^{230}Th equilibrium, the magnetite separate displays strong disequilibrium, immediately indicating that magnetite crystallized significantly less than 8 kyr ago (Fig. 6). More specifically, as Ra partitioning into magnetite is extremely small (Blundy & Wood 2003), all ^{226}Ra can essentially be regarded as ingrown from ^{230}Th (Rubin & Zellmer 2009). A (^{226}Ra/^{230}Th) activity ratio of 0.447 $\pm$ 0.005 (2σ) in the magnetite separate then translates to a ^{226}Ra–^{230}Th age of only 1367 $\pm$ 11 years (2σ) (cf. Fig. 6). This is, of course, much younger than the ages inferred from the U–Th isotochrons. The U–Th and Ra–Th age dichotomy can be reconciled if some proportion of the Shamao dome crystals is older and inherited (i.e. in Ra–Th equilibrium) and some proportion grew just prior to eruption (i.e. with Ra–Th disequilibrium). Although, at face value, the Ra–Th isochron puts the eruption age of the dome into Late Holocene times (<1370 years), just how young the Shamao dome might be depends

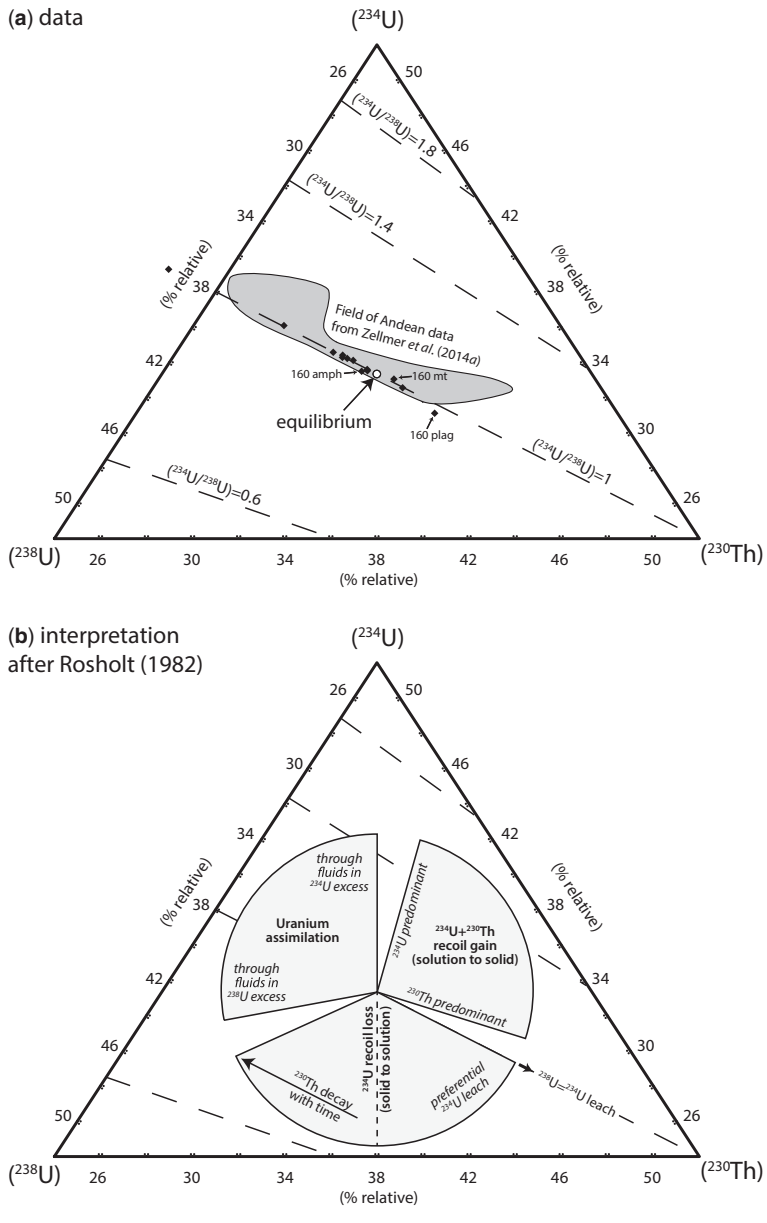

Fig. 7. Triangular diagram of the relative activity proportions of (^{238}U), (^{234}U) and (^{230}Th), after Rosholt (1982). (**a**) Tatun data, with uncertainties smaller than the symbol size. Mineral separates from Mt Cising (sample #160) are indicated, as is the range of data from some recently studied Andean lava flows (Zellmer *et al.* 2014*a*). (**b**) Interpretation of deviations from the point equilibrium (Rosholt 1982), see the text for the discussion.

on the proportion and age of the inherited crystals. For example, if 20% of the magnetite crystals were inherited from an older crustal intrusive body (in ^{226}Ra–^{230}Th secular equilibrium), then the actual eruption age of the dome would decrease to about 800 years BP. Further detailed analytical work on ^{226}Ra and Ba concentrations in other mineral phases from the Shamao dome would be required to extract more precise age constraints on Shamao crystallization ages (cf. Rubin & Zellmer 2009). The extent of the age discordance with a much older Ar–Ar age of 0.20 $\pm$ 0.01 Ma suggests

that some of the inherited crystals may, indeed, be much older, and likely derive from the Miocene basement underlying the area (cf. Belousov *et al.* 2010). It also suggests a significant inherited ^{40}Ar component in the magmas. A Late Holocene eruption age for the Shamao dome has significant implications for volcanic-hazard characterization at the Tatun volcano, with extrusive activity clearly extending into the most recent past.

Turning to Mt Huangzuei (Fig. 5b), similar arguments apply with respect to the crystallization of minerals from the melt v. uptake of minerals into the melt. Distinctly different magnetite–wr/gm and plagioclase–wr/gm ages indicate that these two mineral phases did not crystallize at the same time from the same melt. Thus, it is likely that at least the magnetite assemblage is dominated by earlier formed crystals that were cannibalized by the Mt Huangzuei magma prior to, or at the onset of, eruption. Thus, 72 ± 4 ka (2σ) represents the maximum eruption age of flow #5 of Huangzuei volcano. It should be stressed that the actual eruption of this flow, just like in the case of the Shamao dome, may have occurred much more recently if both plagioclase and magnetite do, in fact, contain a proportion of antecrystic grains that were picked up by the melt at the onset of eruption. The extent of the discordance with the K–Ar age of 0.22 ± 0.02 Ma previously obtained for the Huangzuei lavas (Tsao 1994) suggests that some of their crystal cargo is much older. Additional ^{226}Ra–^{230}Th work will be required to see whether the Huangzuei flow (as well as potentially other morphologically young volcanic edifices of the TVG) may, in fact, be of Holocene age: in which case, both K–Ar and U–Th data would yield significant overestimates on eruption ages. Either way, our analysis provides clear evidence that the TVG can be considered as volcanically active on the basis of its recent explosive and effusive eruption history.

Concluding remarks

The notion of open-system processes in mafic–intermediate composition volcanoes in the subduction zone environment is now well established. Remobilization of shallow intrusives by fresh melt from greater depth is a common phenomenon for porphyritic lava domes (cf. Zellmer 2008, 2009; Kent 2014 and references therein), and some of the Tatun domes and viscous lava flows appear to conform to this petrogenetic scenario. As U–Th internal dating of major mineral phases is not possible on single mineral grains, but instead requires the analysis of bulk mineral separates, the obtained ages are likely to represent averages of a range of ages displayed by the mineral grains (cf. Turner *et al.* 2003). Given the long volcanic history of Tatun volcano, some of the cannibalized mineral grains may have been older than about 350 ka and thus in ^{238}U–^{230}Th–^{226}Ra secular equilibrium. In this case, young bulk separate U–Th internal ages of the order of tens of thousands of years would be likely to contain a number of magnetite grains that are significantly younger, and potentially as young as hundreds of years BP, as demonstrated here by the large ^{226}Ra–^{230}Th disequilibria in the Shamao dome magnetite separates. A suggestion of potentially several voluminous effusive eruptions from the Tatun Volcano Group as recently as Holocene times is thus not too far fetched, and may be detectable through additional analysis of shorter-lived radionuclides such as ^{226}Ra on other morphologically young volcanic deposits.

In conclusion, our study has significant implications for volcanic hazard mitigation strategies at Tatun Volcano Group and elsewhere. We have shown that it is critical to obtain ^{226}Ra–^{230}Th ages in order to check for Holocene volcanic activity even if K–Ar, Ar–Ar or U–Th data yield significantly older ages. Uptake of older crystals is a common phenomenon at arc volcanoes, affects all of the above dating schemes and can only be identified if several dating methods are employed on the same deposits. For volcanic hazard characterization in Taiwan, our data clearly show that the TVG needs to be considered active. This has to be taken into account during planning and mitigation scenarios of major infrastructure in this highly populated area, including nuclear power plants that are situated just a few kilometrer from the longest TVG lava flows.

GFZ thanks Kostas Konstantinou, Kuo-Lung Wang and Tzen-Fu Yui for scientific discussions, and Rong-Yi Yan for sample processing during the early stages of this project. We thank Denys Vonderhaar for assistance with Th–U–Ra chemistry on samples. This manuscript was improved by the constructive comments of Tetsuya Yokoyama and an anonymous reviewer, and the helpful editorial suggestions of Jon Blundy. GFZ acknowledges a Massey University research grant. KHR and JGS acknowledge funding through the United States National Science Foundation (grant EAR-0838271) and the National Science Council of Taiwan (grant 102-2628-M-003-001-MY4), respectively.

References

Arculus, R. J. 2003. Use and abuse of the terms calcalkaline and calcalkalic. *Journal of Petrology*, **44**, 929–935.

Belousov, A., Belousova, M., Chen, C. H. & Zellmer, G. F. 2010. Deposits, character and timing of recent eruptions and large-scale collapses in Tatun Volcanic

Group, Northern Taiwan: hazard-related issues. *Journal of Volcanology and Geothermal Research*, **191**, 205–221.

Blundy, J. & Wood, B. 2003. Mineral–melt partitioning of uranium, thorium and their daughters. *In*: Bourdon, B., Henderson, G. M., Lundstrom, C. C. & Turner, S. P. (eds) *Uranium-Series Geochemistry*. Mineralogical Society of America, Reviews in Mineralogy and Geochemistry, **52**, 59–123.

Bourdon, B., Zindler, A. & Wörner, G. 1994. Evolution of the Laacher See magma chamber: evidence from SIMS and TIMS measurements of U–Th disequilibria in minerals and glasses. *Earth and Planetary Science Letters*, **126**, 75–90.

Cheng, H., Lawrence Edwards, R. *et al.* 2013. Improvements in ^{230}Th dating, ^{230}Th and ^{234}U half-life values, and U–Th isotopic measurements by multi-collector inductively coupled plasma mass spectrometry. *Earth and Planetary Science Letters*, **371–372**, 82–91.

Condomines, M., Gauthier, P.-J. & Sigmarsson, O. 2003. Timescales of magma chamber processes and dating of young volcanic rocks. *In*: Bourdon, B., Henderson, G. M., Lundstrom, C. C. & Turner, S. P. (eds) *Uranium-Series Geochemistry*. Mineralogical Society of America, Reviews in Mineralogy and Geochemistry, **52**, 125–174.

Davidson, J. P., Morgan, D. J. & Charlier, B. L. A. 2007. Frontiers in textural and microgeochemical analysis: isotopic microsampling of magmatic rocks. *Elements*, **3**, 253–259.

Defant, M. J. & Drummond, M. S. 1990. Derivation of some modern arc magmas by melting of young subducted lithosphere. *Nature*, **347**, 662–665.

Dungan, M. A. 2005. Partial melting at the earth's surface: implications for assimilation rates and mechanisms in subvolcanic intrusions. *Journal of Volcanology and Geothermal Research*, **140**, 193–203.

Gill, J. B. 1981. *Orogenic Andesites and Plate Tectonics*. Springer, Heidelberg.

Hoffmann, D. L., Prytulak, J., Richards, D. A., Elliott, T., Coath, C. D., Smart, P. L. & Scholz, D. 2007. Procedures for accurate U and Th isotope measurements by high precision MC–ICPMS. *International Journal of Mass Spectrometry*, **264**, 97–109.

Jaffey, A. H., Flynn, K. F., Glendenin, L. E., Bentley, W. C. & Essling, A. M. 1971. Precision measurement of half-lives and specific activities of ^{235}U and ^{238}U. *Physical Reviews*, **C4**, 1889–1906.

Jerram, D. A. & Martin, V. M. 2008. Understanding crystal populations and their significance through the magma plumbing system. *In*: Annen, C. & Zellmer, G. F. (eds) *Dynamics of Crustal Magma Transfer, Storage and Differentiation*. Geological Society, London, Special Publications, **304**, 133–148, http://doi.org/10.1144/SP304.7

Kent, A. J. R. 2014. Preferential eruption of andesitic magma: implications for volcanic magma fluxes at convergent margins. *In*: Gomez-Tuena, A., Straub, S. M. & Zellmer, G. F. (eds) *Orogenic Andesites and Crustal Growth*. Geological Society, London, Special Publications, **385**, 257–280, http://doi.org/10.1144/SP385.10

Kim, K. H., Chang, C. H., Ma, K. F., Chiu, J. M. & Chen, K. C. 2005. Modern seismic observations in the Tatun volcano region of Northern Taiwan: Seismic/Volcanic Hazard adjacent to the Taipei Metropolitan area. *TAO*, **16**, 579–594.

Konstantinou, K. I. 2015. Potential for future eruptive activity in Taiwan and vulnerability to volcanic hazards. *Natural Hazards*, **75**, 2653–2671, http://doi.org/10.1007/s11069-014-1453-4

Konstantinou, K. I., Lin, C.-H. & Liang, W.-T. 2007. Seismicity characteristics of a potentially active Quaternary volcano: the Tatun Volcano Group, Northern Taiwan. *Journal of Volcanology and Geothermal Research*, **160**, 300–318.

Lee, H.-F., Yang, T. F., Lan, T. F., Song, S.-R. & Tsao, S. 2005. Fumarolic gas composition of the Tatun Volcano Group, Northern Taiwan. *TAO*, **16**, 843–864.

Lee, H.-F., Yang, T. F., Lan, T. F., Song, S.-R. & Tsao, S. 2008. Temporal variations of gas compositions of fumaroles in the Tatun Volcano Group, Northern Taiwan. *Journal of Volcanology and Geothermal Research*, **178**, 624–635.

Lee, S. F. 1996. *Volcanic sequence study of the Tatun Volcano Group: the Chihsinshan subgroup*. MSc thesis, National Taiwan University (in Chinese).

Lin, C. H., Konstantinou, K. I., Liang, W. T., Pu, H. C., Lin, Y. M., You, S. H. & Huang, Y. P. 2005. Preliminary analysis of volcanoseismic signals recorded at the Tatun Volcano Group, Northern Taiwan. *Geophysical Research Letters*, **32**, L10313.

Peacock, M. A. 1931. Classification of igneous rock series. *Journal of Geology*, **39**, 54–67.

Peccerillo, A. & Taylor, S. R. 1976. Geochemistry of Eocene calc-alkaline volcanic rocks from the Kastamonu area, northern Turkey. *Contributions to Mineralogy and Petrology*, **58**, 63–81.

Pietruszka, A. J., Carlson, R. W. & Hauri, E. K. 2002. Precise and accurate measurements of ^{226}Ra–^{230}Th–^{238}U disequilibrium in volcanic rocks using plasma ionization multicollector mass spectrometry. *Chemical Geology*, **188**, 171–191.

Pyle, D. M., Ivanovich, M. & Sparks, R. S. J. 1988. Magma cumulate mixing identified by U–Th disequilibrium dating. *Nature*, **331**, 157–159.

Richter, S., Eykens, R., Kuehn, H., Aregbe, Y., Verbruggen, A. & Weyer, S. 2010. New average values for the $n(^{238}U)/n(^{235}U)$ isotope ratios of natural uranium standards. *International Journal of Mass Spectrometry*, **295**, 94–97.

Rosholt, J. N. 1982. Mobilization and weathering. *In*: Ivanovich, M. & Harmon, R. S. (eds) *Uranium Series Disequilibrium: Applications to Environmental Problems*. Clarendon Press, Oxford, 167–180.

Rubin, K. H. 2001. Analysis of ^{232}Th/^{230}Th in volcanic rocks: a comparison of Thermal Ionization Mass Spectrometry and other methodologies. *Chemical Geology*, **175**, 755–782.

Rubin, K. H. & Zellmer, G. F. 2009. Reply to comment on 'on the recent bimodal magmatic processes and their rates in the Torfajökull–Veidivötn area, Iceland' by K. M. Cooper. *Earth and Planetary Science Letters*, **281**, 115–123.

Rubin, K. H., van der Zander, I., Smith, M. C. & Bergmanis, E. C. 2005. Minimum speed limit for ocean

ridge magmatism from $^{210}Pb-^{226}Ra-^{230}Th$ disequilibria. *Nature*, **437**, 534–538.

SHELLNUTT, J. G., BELOUSOV, A., BELOUSOVA, M., WANG, K. L. & ZELLMER, G. F. 2014. Generation of calc-alkaline andesite of the Tatun volcanic group (Taiwan) within an extensional environment by crystal fractionation. *International Geology Review*, **56**, 1156–1171.

SONG, S.-R., YANG, T. F., YEH, Y.-H., TSAO, S.-J. & LO, H.-J. 2000. The Tatun volcano group is active or extinct? *Journal of the Geological Society of China*, **43**, 521–534.

STEWART, R. B., PRICE, R. C. & SMITH, I. E. M. 1996. Evolution of high-K arc magma, Egmont volcano, Taranaki, New Zealand: evidence from mineral chemistry. *Journal of Volcanology and Geothermal Research*, **74**, 275–295.

STRECK, M. J., LEEMAN, W. P. & CHESLEY, J. 2007. High-magnesian andesite from Mount Shasta: a product of magma mixing and contamination, not a primitive mantle melt. *Geology*, **35**, 351–354.

SUN, S. S. & MCDONOUGH, W. F. 1989. Chemical and isotopic systematics of oceanic basalts: implications for mantle composition and processes. *In*: SAUNDERS, A. D. & NORRY, M. J. (eds) *Magmatism in Ocean Basins*. Geological Society, London, Special Publications, **42**, 313–345, http://doi.org/10.1144/GSL.SP.1989.042.01.19

TSAO, S. 1994. K–Ar age determination of volcanic rocks from the Tatun Volcano Group. *Bulletin of the Central Geological Survey*, **9**, 137–154 (in Chinese).

TURNER, S. P., GEORGE, R. M. M., EVANS, P. J., HAWKESWORTH, C. J. & ZELLMER, G. F. 2000. Time-scales of magma formation, ascent and storage beneath subduction-zone volcanoes. *Philosophical Transactions of the Royal Society of London A*, **358**, 1443–1464.

TURNER, S. P., GEORGE, R. M. M., JERRAM, D. A., CARPENTER, N. & HAWKESWORTH, C. J. 2003. Case studies of plagioclase growth and residence times in island arc lavas from Tonga and the Lesser Antilles, and a model to reconcile discordant age information. *Earth and Planetary Science Letters*, **214**, 279–294.

WANG-LEE, C. M., CHENG, Y. M. & WANG, Y. 1978. Geological and sedimentary study. *Taiwan Mineral Industry*, **30**, 78–108.

WANG, K. L., CHUNG, S. L., O'REILLY, S. Y., SUN, S. S., SHINJO, R. & CHEN, C. H. 2004. Geochemical constraints for the genesis of post-collisional magmatism and the geodynamic evolution of the northern Taiwan region. *Journal of Petrology*, **45**, 975–1011.

WITT, M. L. I., FISCHER, T. P., PYLE, D. M., YANG, T. F.& ZELLMER, G. F. 2008. In-situ gas composition measurements in the plume of Tatun Volcano, Taiwan: comparison to direct sampling of fumaroles. *Journal of Volcanology and Geothermal Research*, **178**, 636–643.

YANG, T. F., SANO, Y. & SONG, S.-R. 1999. $^{3}He/^{4}He$ ratios of fumaroles and bubbling gases of hot springs in Tatun Volcano Group, North Taiwan. *Il Nuovo Cimento*, **22C**, 281–286.

YU, S. B., CHEN, H. Y. & KUO, L. C. 1997. Velocity field of GPS stations in the Taiwan area. *Tectonophysics*, **274**, 41–59.

ZELLMER, G. F. 2008. Some first order observations on magma transfer from mantle wedge to upper crust at volcanic arcs. *In*: ANNEN, C. & ZELLMER, G. F. (eds) *Dynamics of Crustal Magma Transfer, Storage and Differentiation*. Geological Society, London, Special Publications, **304**, 15–31, http://doi.org/10.1144/SP304.2

ZELLMER, G. F. 2009. Petrogenesis of Sr-rich adakitic rocks at volcanic arcs: insights from global variations of eruptive style with plate convergence rates and surface heat flux. *Journal of the Geological Society, London*, **166**, 725–734.

ZELLMER, G. F., ANNEN, C., CHARLIER, B. L. A., GEORGE, R. M. M., TURNER, S. P. & HAWKESWORTH, C. J. 2005. Magma evolution and ascent at volcanic arcs: constraining petrogenetic processes through rates and chronologies. *Journal of Volcanology and Geothermal Research*, **140**, 171–191.

ZELLMER, G. F., RUBIN, K. H., GRÖNVOLD, K. & JURADO-CHICHAY, Z. 2008. On the recent bimodal magmatic processes and their rates in the Torfajökull–Veidivötn area, Iceland. *Earth and Planetary Science Letters*, **269**, 387–397.

ZELLMER, G. F., FREYMUTH, H., CEMBRANO, J. M., CLAVERO, J. E., VELOSO, E. A. E. & SIELFELD, G. G. 2014*a*. Altered mineral uptake into fresh arc magmas: insights from U–Th isotopes of samples from Andean volcanoes under differential crustal stress regimes. *In*: GOMEZ-TUENA, A., STRAUB, S. M. & ZELLMER, G. F. (eds) *Orogenic Andesites and Crustal Growth*. Geological Society, London, Special Publications, **385**, 185–208, http://doi.org/10.1144/SP385.9

ZELLMER, G. F., HWANG, S.-L. *ET AL.* 2014*b*. Interaction of arc magmas with subvolcanic hydrothermal systems: insights from compositions and metasomatic textures of olivine crystals in fresh basalts of Daisen and Mengameyama, Western Honshu, Japan. *In*: ZELLMER, G. F., EDMONDS, M. & STRAUB, S. M. (eds) *The Role of Volatiles in the Genesis, Evolution and Eruption of Arc Magmas*. Geological Society, London, Special Publications, **410**, 219–236, http://doi.org/10.1144/SP410.1

ZELLMER, G. F., SAKAMOTO, N., IIZUKA, Y., MIYOSHI, M., TAMURA, Y., HSIEH, H.-H. & YURIMOTO, H. 2014*c*. Crystal uptake into aphyric arc melts: insights from two-pyroxene pseudo-decompression paths, plagioclase hygrometry, and measurement of hydrogen in olivines from mafic volcanics of southwest Japan. *In*: GOMEZ-TUENA, A., STRAUB, S. M. & ZELLMER, G. F. (eds) *Orogenic Andesites and Crustal Growth*. Geological Society, London, Special Publications, **385**, 161–184, http://doi.org/10.1144/SP385.3